J. Non-Newtonian Fluid Mech. 159 (2009) 72–80

Contents lists available at ScienceDirect

Journal of Non-Newtonian Fluid Mechanics

journal homepage: www.elsevier.com/locate/jnnfm

An adaptive mixed least-squares finite element method for viscoelastic fluids of Oldroyd type☆

Z. Cai[a], C.R. Westphal[b,*]

[a] Department of Mathematics, Purdue University, 150 N. University St., West Lafayette, IN 47907-2067, United States
[b] Department of Mathematics and Computer Science, Wabash College, 301 W. Wabash, Crawfordsville, IN 47933, United States

ARTICLE INFO

Article history:
Received 25 June 2008
Received in revised form 21 January 2009
Accepted 5 February 2009

Keywords:
Viscoelastic fluid
Oldroyd
Least-squares
Raviart–Thomas
Finite element
Adaptive mesh refinement
Corner singularities
4:1 contraction

ABSTRACT

We present a new least-squares finite element method for the steady Oldroyd type viscoelastic fluids. The overall iterative procedure combines a nonlinear nested iteration, where adaptive mesh refinement is based on a nonlinear least-squares functional. Each linear step is solved by a least-squares finite element minimization. The homogeneous least-squares functional is shown to be equivalent to a natural norm, and, under sufficient smoothness assumptions, finite element error bounds are shown to be optimal when using conforming piecewise polynomial elements for the velocity, pressure and extra stress, and Raviart–Thomas finite elements for the total stress. In the absence of full regularity, a local weighted-norm approach is used to remove effects of corner singularities. Numerical results are given for an Oldroyd-B fluid in a 4:1 contraction, showing optimal reduction of the least-squares functional.

© 2009 Elsevier B.V. All rights reserved.

1. Introduction

While much progress has been made in recent years toward the accurate and efficient simulation of viscoelastic fluids under differential constitutive laws, many difficulties persist. We consider the solution to steady Oldroyd systems, where, in contrast to Newtonian models, the stress cannot be eliminated to form a single second-order equation in terms of the velocity and pressure. In general, the stress must be directly approximated.

As the Weissenberg number increases, the constitutive equation exhibits dominant convective behavior and the nonlinear coupling between the unknowns increases. One major difficulty in the simulation of viscoelastic fluids is the failure of the nonlinear iteration to converge at some threshold in the Weissenberg number. Thus, it is critically important to design a method that is robust with respect to the nonlinear solver. Nonsmooth boundaries can introduce singularities which, if left unaddressed, may cause significant degradation of numerical methods, or worse, may even contribute to the failure of the nonlinear iteration. In fact, near reentrant corners the extra stress may not be in $H^1(\Omega)$, a major difficulty for using finite element subspaces of $H^1(\Omega)$. Finally, the algebraic systems that must be solved from typical discretizations are difficult to handle and require the use of efficient iterative solvers. The properties of the resulting algebraic systems should be considered closely in the design of the discretization to ensure an efficient numerical method.

The analytical and numerical study of viscoelastic fluids has developed a rich history, distinguished by contributions to industrial applications as well as providing a generalization to classical fluid mechanics. This range is reflected in works [34,35,2,21,37].

In [39] Wang and Carey introduced a least-squares approach to upper-convected Maxwell (UCM) fluids and in [5] Bose and Carey gave a more sophisticated approach for UCM and Bingham fluids, utilizing mesh redistribution and polynomial refinement to handle problems due to boundary singularities. Gerritsma, in [23], used a discontinuous least-squares spectral element approach for UCM fluids. This paper is similar in general approach to these papers, but provides a novel approach to the nonlinear iteration, treatment of boundary singularities, and adaptive mesh refinement. Also, to our knowledge, this paper is the first to prove least-squares functional ellipticity results and rigorous error bounds for linearized viscoelastic fluids. The theory we present here includes the Oldroyd models in two or three dimensions and also includes the inertial terms in the balance of momentum equations.

☆ This work was sponsored by the National Science Foundation under grant DMS–0511430.

* Corresponding author.
E-mail addresses: zcai@math.purdue.edu (Z. Cai), westphac@wabash.edu, loschados@yahoo.com (C.R. Westphal).

0377-0257/$ – see front matter © 2009 Elsevier B.V. All rights reserved.
doi:10.1016/j.jnnfm.2009.02.004

The least-squares finite element method is based on an explicit minimization principle to form a symmetric variational problem. In recent years, least-squares methods have been developed and refined for many applications in continuum mechanics. See for example general references [26,4,7,10], works on fluids [11,12,28,8,3], or works on solid mechanics [13,14,38,9,32]. The least-squares approach displays several attractive features for such problems. In its most basic form, a least-squares method is formed by minimizing the norm of the residual of the equations over a solution space compatible with the exact solution. An appropriate formulation of the equations and choice of norms to minimize over ensures that the error is efficiently reduced in a meaningful norm. The locally evaluated least-squares functional can then serve as a reliable and inexpensive error estimator, which can be used in adaptive refinement strategies. Further, a strong advantage of the method is that it always produces symmetric, positive definite linear systems that can generally be solved with optimal complexity with standard multigrid methods. It is also worth noting that the least-squares approach here is not the same as the Galerkin Least Squares (GLS) approach.

Nonlinear PDE problems can be approached by linearizing the equations first and then applying a least-squares method to the linear equations, or by forming a nonlinear variational problem and then linearizing the resulting equations. In this paper, we use the former approach and note that it is not clear which is more effective for difficult nonlinearities. In this paper, we combine the use of a least-squares discretization with a nonlinear nested iteration. That is, the nonlinear iteration is done in tandem with mesh refinement. At each linearzation step, a nonlinear functional serves as an indicator to decide when to interpolate a current solution to a finer mesh. This not only produces a more efficient iteration by performing the earlier linearization steps with coarser resolution, but it also provides good initial guesses for the finer meshes, producing a more robust nonlinear iteration.

As are many finite element methods, least-squares methods are sensitive to a loss of regularity due to nonsmooth boundaries, thus, care must be taken in this respect. In the presence of such singularities, our approach replaces the L^2 norms in the least-squares functional with locally weighted norms, which eliminates the pollution effect and improves discretization accuracy. Details of this approach can be seen in [29,30,18,15].

The organization of this paper is as follows. Section 2 introduces the notation we use and the equations we consider. Section 3 describes the nonlinear iteration, the function spaces for the unknowns and the adaptive refinement procedure. The least-squares minimization is detailed and the ellipticity of the least-squares functional is proved in Section 4. In Section 5 the finite element spaces are discussed and optimal error bounds are proved. Section 6 provides details of the weighted-norm treatment of boundary singularities, and numerical results are given in Section 7.

2. Notation and equations

We use standard notation for Sobolev spaces $H^k(\Omega)^d$ and corresponding norm $\|\cdot\|_{k,\Omega}$ for $k \geq 0$. We drop subscript Ω and superscript d when the domain and dimension are clear by context. For noninteger k, $H^k(\Omega)$ is the interpolation space between $H^{\lfloor k\rfloor}(\Omega)$ and $H^{\lceil k\rceil}(\Omega)$ as in [31]. The case of $k = 0$ corresponds to the Lebesgue measurable space, $L^2(\Omega)$, in which case we generally denote the norm and inner product by $\|\cdot\|$ and $\langle\cdot,\cdot\rangle$, respectively. Define the subspace of $L^2(\Omega)^d$ induced by the divergence of $\mathbf{u}$ by

$$H(\mathrm{div}) = \{\mathbf{u} \in L^2(\Omega)^d : \|\nabla\cdot\mathbf{u}\| < \infty\},$$

with norm satisfying

$$\|\mathbf{u}\|^2_{H(\mathrm{div})} = \|\mathbf{u}\|^2 + \|\nabla\cdot\mathbf{u}\|^2.$$

The divergence and trace of $d\times d$ tensor $\boldsymbol{\tau}$ are given by $(\nabla\cdot\boldsymbol{\tau})_i = \sum_{j=1}^d \partial\tau_{ij}/\partial x_j$ and $\mathrm{tr}(\boldsymbol{\tau}) = \sum_{i=1}^d \tau_{ii}$. The space of tensor valued functions with each row in $H(\mathrm{div})$ is denoted by $H(\mathrm{div})^d$. We also define the operator $\mathbf{u}\cdot\nabla = \sum_{k=1}^d u_k\partial/\partial x_k$ so that for each $i,j = 1,\ldots,d$ we have $(\mathbf{u}\cdot\nabla\mathbf{u})_i = \sum_{k=1}^d u_k\partial u_i/\partial x_k$ and $(\mathbf{u}\cdot\nabla\boldsymbol{\tau})_{ij} = \sum_{k=1}^d u_k\partial\tau_{ij}/\partial x_k$.

The conservation of mass and momentum equations for time-dependent incompressible flow are given by

$$\nabla\cdot\mathbf{u} = 0, \quad \text{and} \quad \rho\left(\frac{\partial\mathbf{u}}{\partial t} + \mathbf{u}\cdot\nabla\mathbf{u}\right) - \nabla\cdot\boldsymbol{\sigma} = \tilde{\mathbf{f}}, \tag{1}$$

where ρ is the fluid density, $\tilde{\mathbf{f}}$ is an internal body force and the unknowns $\mathbf{u}$ and $\boldsymbol{\sigma}$ are the velocity vector and the stress tensor, respectively.

System (1) must be closed by a constitutive equation. In this paper we consider a general Oldroyd fluid, where an elastic material of viscosity μ_1 is dissolved in a viscous solvent of viscosity μ_2. The total stress has elastic and solvent components, $\boldsymbol{\tau}$ and $\boldsymbol{\tau}_s$, respectively, which satisfy

$$\boldsymbol{\sigma} = \boldsymbol{\tau} + \boldsymbol{\tau}_s - p\mathbf{I},$$

where p is the pressure and $\mathbf{I}$ is the $d\times d$ identity tensor. The solvent stress satisfies

$$\boldsymbol{\tau}_s = 2\mu_2\boldsymbol{\epsilon}(\mathbf{u}),$$

where $\boldsymbol{\epsilon}(\mathbf{u}) = (1/2)(\nabla\mathbf{u} + \nabla\mathbf{u}^t)$ is the standard strain rate tensor. The symmetric elastic stress satisfies

$$\boldsymbol{\tau} + \lambda\left(\frac{\partial\boldsymbol{\tau}}{\partial t} + \mathbf{u}\cdot\nabla\boldsymbol{\tau} + g_a(\nabla u,\boldsymbol{\tau})\right) = 2\mu_1\boldsymbol{\epsilon}(\mathbf{u}),$$

where λ is a characteristic stress relaxation time for the fluid and

$$g_a(\nabla u,\boldsymbol{\tau}) = \frac{1-a}{2}((\nabla\mathbf{u})\boldsymbol{\tau} + \boldsymbol{\tau}(\nabla\mathbf{u})^t) - \frac{1+a}{2}(\boldsymbol{\tau}(\nabla\mathbf{u}) + (\nabla\mathbf{u})^t\boldsymbol{\tau})$$

is a bilinear tensor-valued function, depending on the parameter $a\in[-1,1]$.

We nondimensionalize the equations by scaling the lengths by L, the velocities by V, time by L/V, and the stresses by $\mu V/L$, where $\mu \equiv \mu_1+\mu_2$ is the total viscosity. Further, we define $\mathcal{R}\rceil \equiv \rho VL/\mu$, $\mathcal{W}\rceil \equiv \lambda V/L$, and $\omega \equiv \mu_1/\mu \in [0,1]$ as the dimensionless Reynolds number, Weissenberg number and retardation parameter, respectively. This general viscoelastic model is characterized by the four parameters $\mathcal{R}\rceil$, $\mathcal{W}\rceil$, a and ω and can be written as

$$\begin{cases} \nabla\cdot\mathbf{u} = 0 & \text{in } \Omega,\\ \mathcal{R}\rceil\left(\dfrac{\partial\mathbf{u}}{\partial t} + \mathbf{u}\cdot\nabla\mathbf{u}\right) - \nabla\cdot\boldsymbol{\sigma} = \hat{\mathbf{f}} & \text{in } \Omega,\\ \boldsymbol{\sigma} - \boldsymbol{\tau} + p\mathbf{I} - 2(1-\omega)\boldsymbol{\epsilon}(\mathbf{u}) = \mathbf{0} & \text{in } \Omega,\\ \boldsymbol{\tau} + \mathcal{W}\rceil\left(\dfrac{\partial\boldsymbol{\tau}}{\partial t} + \mathbf{u}\cdot\nabla\boldsymbol{\tau} + g_a(\nabla\mathbf{u},\boldsymbol{\tau})\right) - 2\omega\boldsymbol{\epsilon}(\mathbf{u}) = \mathbf{0} & \text{in } \Omega,\\ \mathbf{u} = \mathbf{0} & \text{on } \partial\Omega, \end{cases} \tag{2}$$

where for simplicity of presentation, homogeneous boundary conditions are assumed on $\partial\Omega$. Nonhomogeneous velocity boundary conditions can be treated analogously, but our present analysis is restricted to pure Dirichlet type boundary conditions. System (2) represents unknowns $\mathbf{u}$, p, $\boldsymbol{\sigma}$, and $\boldsymbol{\tau}$. In general, least-squares methods involve an appropriate first-order system of PDEs, often formed by introducing new unknowns to a second-orderPDE.

Often, as in this paper, the unknowns are chosen to be physically relevant.

The Oldroyd-A and B models correspond to $a = 1$ and $a = -1$, respectively, and the Maxwell model corresponds to $\omega = 1$ (the upper-convected Maxwell model has $a = -1$ and the lower-convected Maxwell model has $a = 1$). The Newtonian model corresponds to $\omega = 0$, and in this viscous limit, the stresses can be eliminated by substitution into the momentum equation, resulting in the standard Navier–Stokes model. We assume throughout that $\omega \in (0, 1)$.

In this paper we consider the steady-state model by dropping the time derivatives. The analysis here may also be generalized to the dynamic problem for many implicit time-marching or operator splitting schemes, where at each time step, the system is similar to the system we consider, but with the addition of lower order terms in $\mathbf{u}$ and $\boldsymbol{\tau}$.

3. Nonlinear iterative method

Our solution method couples adaptive mesh refinement with an inexact Newton iteration. Each intermediate, linear step is discretized by minimizing a least-squares finite element functional. In this section, we describe the nonlinear nested iteration in general terms and give criteria for the adaptive refinement. The least-squares step is discussed in detail in Section 4.

For the velocity and pressure, define the spaces

$$\mathbf{V} = \{\mathbf{v} \in H^1(\Omega)^d : \mathbf{v} = 0 \text{ on } \partial\Omega\},$$
$$\mathbf{Q} = L^2(\Omega)/\mathbb{R}.$$

Since for any solution to (2) we have $\mathrm{tr}(\boldsymbol{\epsilon}(\mathbf{u})) = \nabla \cdot \mathbf{u} = 0$, then applying the trace operator to the third equation in (2) results in $\mathrm{tr}(\boldsymbol{\sigma}) = \mathrm{tr}(\boldsymbol{\tau}) - \mathrm{d}p$. Thus $p \in \mathbf{Q}$ may be chosen so that $\int_\Omega p\,\mathrm{d}x = (1/\mathrm{d})\int_\Omega \mathrm{tr}(\boldsymbol{\tau})\,\mathrm{d}x$, which implies that in the case of pure Dirichlet boundary conditions we are free to impose

$$\int_\Omega \mathrm{tr}(\boldsymbol{\sigma})\,\mathrm{d}x = 0.$$

Also, we note that we are free to impose symmetry of $\boldsymbol{\tau}$. We now define spaces for each stress by

$$\mathbf{S} = \{\mathbf{s} \in H(\mathrm{div})^d : \int_\Omega \mathrm{tr}(\mathbf{s})\,\mathrm{d}x = 0\},$$
$$\mathbf{T} = \{\mathbf{t} \in L^2(\Omega)^{d\times d} : \|\mathbf{b}\cdot\nabla\mathbf{t}\| < \infty, \mathbf{t}^t = \mathbf{t}\},$$

where $\mathbf{b} \in H^1(\Omega)^d$ is a known approximation to the velocity. Finally, define the product space $\mathbf{X} = \mathbf{V}\times\mathbf{Q}\times\mathbf{S}\times\mathbf{T}$.

Denote the unknowns by $U = (\mathbf{u}, p, \boldsymbol{\sigma}, \boldsymbol{\tau}) \in \mathbf{X}$ and the steady-state residual of (2) by

$$F(U) := \begin{pmatrix} \nabla\cdot\mathbf{u} \\ \mathcal{R}](\mathbf{u}\cdot\nabla\mathbf{u}) - \nabla\cdot\boldsymbol{\sigma} - \hat{\mathbf{f}} \\ \boldsymbol{\sigma} - \boldsymbol{\tau} + p\mathbf{I} - 2(1-\omega)\boldsymbol{\epsilon}(\mathbf{u}) \\ \boldsymbol{\tau} + \mathcal{W}](\mathbf{u}\cdot\nabla\boldsymbol{\tau} + g_a(\nabla\mathbf{u}, \boldsymbol{\tau})) - 2\omega\boldsymbol{\epsilon}(\mathbf{u}) \end{pmatrix}.$$

We now approximate the solution to $F(U) = 0$ by an inexact Newton iteration. To this end, denote the n^{th} adaptively refined triangulation of Ω by Ω^n, with elements K. The ℓ^{th} iterate approximated on Ω^n is given by U_ℓ^n. Also formally denote $\mathbf{X}^h$ as the corresponding finite dimensional solution space for U_ℓ^n. Precise definitions of the finite element spaces are given in Section 5. Each linear step in this iterative procedure is found by solving for the update $S_\ell^n = U_{\ell+1}^n - U_\ell^n$ in the linear problem

$$J(U_\ell^n)S_\ell^n = -F(U_\ell^n), \tag{3}$$

where J is the Jacobian of F. The new approximation is given by $U_{\ell+1}^n = U_\ell^n + \lambda_\ell S_\ell^n$, where the line search parameter, $\lambda_\ell \in (0, 1)$, is chosen to minimize $F(U_\ell^n + \lambda_\ell S_\ell^n)$. Each linear problem (3) is cast as a least-squares minimization problem by defining the linear least-squares functional

$$G(S_\ell^n) = \|J(U_\ell^n)S_\ell^n + F(U_\ell^n)\|^2, \tag{4}$$

and then finding $S_\ell^n \in \mathbf{X}^h$ such that

$$G(S_\ell^n) \le G(V_\ell^n) \quad \text{for all } V_\ell^n \in \mathbf{X}^h. \tag{5}$$

Following each linear functional minimization, the velocity is projected onto a subspace of approximately divergence-free vectors. By doing this we may assume that the succeeding linearization is done about an approximation that satisfies conservation of mass up to within discretization error on the current mesh. This pseudo-div-free projection is discussed in detail in the next section. In the nonlinear nested iteration algorithm summarized below, this projection step is denoted by *project velocity*.

Define the nonlinear least-squares functional

$$\mathcal{G}(U_\ell^n) = \|F(U_\ell^n)\|^2. \tag{6}$$

To determine approximate convergence of Newton's method on level n, we iterate on k until

$$\mathcal{G}(U_\ell^n) \le (1 + \epsilon_n)G(S_\ell^n), \tag{7}$$

where ϵ_n is a tolerance parameter, potentially dependent on the refinement level, n. When (7) is satisfied, all elements, K, are refined for which

$$\|F(U_\ell^n)\|_K^2 > \mathcal{G}_{\min} + \eta(\mathcal{G}_{\max} - \mathcal{G}_{\min})$$

where $\mathcal{G}_{\min} = \min_K \|F(U_\ell^n)\|_K^2$ and $\mathcal{G}_{\max} = \max_K \|F(U_\ell^n)\|_K^2$ are minimum and maximum local nonlinear functional values and the parameter $\eta \in [0, 1]$ determines how aggressive the mesh refinement is. Generally we choose η so that at least 25% of the elements are refined. Fig. 1 describes the refinement.

When the mesh is refined, the finite element spaces are updated and current approximations are interpolated and redefined relative to the mesh. In Section 7 we consider a model problem and give numerical results of this nonlinear nested iteration where four levels of refinement are used. The overall algorithm is summarized below.

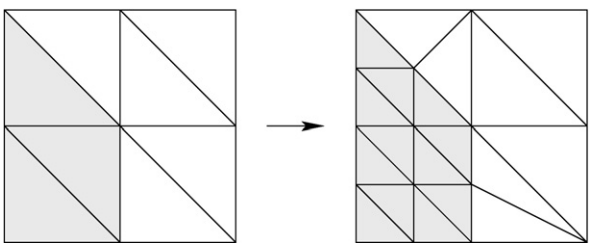

Fig. 1. Detail of mesh refinement: refined elements are split into four smaller elements by bisecting edges, and elements adjacent to a bisected edge are split into two elements.

Nonlinear Nested Iteration Algorithm:

n_{max} = "number of refinement levels";
$U_0^0 = 0$;
Ω^n = "initial coarse discretization of Ω";
for $n = 1, \cdots, n_{max}$, **do**
  $k = 0$;
  while $\mathcal{G}(U_\ell^n) \le (1+\epsilon_n) G(S_\ell^n)$, **do**
    $S_\ell^n = \underset{V_\ell^n \in \mathbf{X}^h}{argmin}\ G(V_\ell^n)$;
    $\lambda_\ell = \underset{\lambda \in [0,1]}{argmin}\ F(U_\ell^n + \lambda S_\ell^n)$;
    $U_{\ell+1}^n = U_\ell^n + \lambda_\ell S_\ell^n$;
    project velocity;
    $\ell = \ell + 1$;
  end while
  if $n \neq n_{max}$, **do**
    $\Omega^{n+1} = \text{refine}(\Omega^n)$;
    update $\mathbf{X}^h$ relative to Ω^{n+1};
    $U_0^{n+1} = \text{interpolate}(U_\ell^n)$;
  end if
  $n = n + 1$;
end for

A detailed study of convergence of this type of nested iteration is studied in the least-squares context in [17]. Problems with dominant nonlinearities may require many total Newton iterations. Combining the nonlinear iteration with mesh adaptation allows for the initial crude approximations to be carried out on coarse meshes where the computation is inexpensive. By performing sufficient Newton iterations on these coarse meshes, the nonlinear error is resolved to the level of discretization error and the finer meshes generally require only a small number of linear steps. This not only results in a computationally efficient algorithm, but producing good initial guesses for the finer meshes seems to expand the basin of attraction of Newton's method. Using locally evaluated functionals as an error indicator is also a topic of study in [16].

In this paper we treat the nonlinearity on the continuous level, that is, we construct the Newton iteration based on the equations before discretization. In contrast to this approach, we note that it is possible to discretize a nonlinear least-squares functional, resulting in a nonlinear system of algebraic equations to which variants of Newton's method may be applied. Our approach, however, admits symmetric positive definite linear algebraic systems, which are efficiently solved by an appropriate iterative method such as a multigrid preconditioned conjugate gradient method. Though our emphasis for the present is to analyze the linearized system, the key to an overall efficient method is to identify and balance the distinct components of error: nonlinear, discretization, and algebraic.

4. Least-squares minimization

We now describe the specific form of each linear system (3) and describe more completely the least-squares functional (4) and associated minimization problem (5).

Linearizing (2) about the current approximation

$$\boldsymbol{\beta} \approx \boldsymbol{\tau}, \qquad \mathbf{b} \approx \mathbf{u},$$

where we assume $\nabla \cdot \mathbf{b} = 0$ and

$$\max\{\|\mathbf{b}\|_\infty, \|\nabla \mathbf{b}\|_\infty, \|\boldsymbol{\beta}\|_\infty, \|\nabla \boldsymbol{\beta}\|_\infty\} \le M < \infty, \tag{8}$$

results in the following replacement rules:

$$\begin{aligned}
&\mathbf{u}\cdot\nabla\mathbf{u} \to \mathbf{b}\cdot\nabla\mathbf{u} + \mathbf{u}\cdot\nabla\mathbf{b} - \mathbf{b}\cdot\nabla\mathbf{b},\\
&\mathbf{u}\cdot\nabla\boldsymbol{\tau} \to \mathbf{b}\cdot\nabla\boldsymbol{\tau} + \mathbf{u}\cdot\nabla\boldsymbol{\beta} - \mathbf{b}\cdot\nabla\boldsymbol{\beta},\\
&g_a(\nabla\mathbf{u}, \boldsymbol{\tau}) \to g_a(\nabla\mathbf{b}, \boldsymbol{\tau}) + g_a(\nabla\mathbf{u}, \boldsymbol{\beta}) - g_a(\nabla\mathbf{b}, \boldsymbol{\beta}).
\end{aligned}$$

The linearized system may now be written as

$$\begin{cases}
\nabla\cdot\mathbf{u} = 0 & \text{in } \Omega,\\
\mathcal{R}e(\mathbf{b}\cdot\nabla\mathbf{u} + \mathbf{u}\cdot\nabla\mathbf{b}) - \nabla\cdot\boldsymbol{\sigma} = \mathbf{f} & \text{in } \Omega,\\
\boldsymbol{\sigma} - \boldsymbol{\tau} + p\mathbf{I} - 2(1-\omega)\boldsymbol{\epsilon}(\mathbf{u}) = \mathbf{0} & \text{in } \Omega,\\
\boldsymbol{\tau} + \mathcal{W}e\mathbf{b}\cdot\nabla\boldsymbol{\tau} + B(\mathbf{u}, \boldsymbol{\tau}) - 2\omega\boldsymbol{\epsilon}(\mathbf{u}) = \mathbf{F} & \text{in } \Omega,\\
\mathbf{u} = \mathbf{0} & \text{on } \partial\Omega,
\end{cases} \tag{9}$$

where we define

$$\begin{aligned}
&\mathbf{f} = \hat{\mathbf{f}} + \mathcal{R}]\mathbf{b}\cdot\nabla\mathbf{b},\\
&B(\mathbf{u}, \boldsymbol{\tau}) = \mathcal{W}](\mathbf{u}\cdot\nabla\boldsymbol{\beta} + g_a(\nabla\mathbf{b}, \boldsymbol{\tau}) + g_a(\nabla\mathbf{u}, \boldsymbol{\beta})),\\
&\mathbf{F} = \mathcal{W}](\mathbf{b}\cdot\nabla\boldsymbol{\beta} + g_a(\nabla\mathbf{b}, \boldsymbol{\beta})).
\end{aligned}$$

The least-squares functional we consider is given by

$$\begin{aligned}
G(\mathbf{u}, p, \boldsymbol{\sigma}, \boldsymbol{\tau}; \mathbf{f}, \mathbf{F}) = {} & \|\nabla\cdot\mathbf{u}\|^2 + \|\mathcal{R}](\mathbf{b}\cdot\nabla\mathbf{u} + \mathbf{u}\cdot\nabla\mathbf{b}) - \nabla\cdot\boldsymbol{\sigma} - \mathbf{f}\|^2\\
&+ \|\boldsymbol{\sigma} - \boldsymbol{\tau} + p\mathbf{I} - 2(1-\omega)\boldsymbol{\epsilon}(\mathbf{u})\|^2\\
&+ \|\boldsymbol{\tau} + \mathcal{W}]\mathbf{b}\cdot\nabla\boldsymbol{\tau} + B(\mathbf{u}, \boldsymbol{\tau}) - 2\omega\boldsymbol{\epsilon}(\mathbf{u}) - \mathbf{F}\|^2.
\end{aligned}$$

We now show equivalence of the norm induced by the homogeneous least-squares functional to the norm

$$|||(\mathbf{u}, p, \boldsymbol{\sigma}, \boldsymbol{\tau})||| = \left(\|\mathbf{u}\|_1^2 + \|p\|^2 + \|\boldsymbol{\sigma}\|_{H(\text{div})}^2 + \|\boldsymbol{\tau}\|^2 + \|\mathbf{b}\cdot\nabla\boldsymbol{\tau}\|^2\right)^{1/2}$$

over $\mathbf{X}$.

Theorem 4.1. *For all $(\mathbf{u}, p, \boldsymbol{\sigma}, \boldsymbol{\tau}) \in \mathbf{X}$, there are positive constants, c_0 and c_1, which depend on Ω, ω, M, $\mathcal{W}]$ and $\mathcal{R}]$, such that*

$$c_0|||(\mathbf{u}, p, \boldsymbol{\sigma}, \boldsymbol{\tau})|||^2 \le G(\mathbf{u}, p, \boldsymbol{\sigma}, \boldsymbol{\tau}; \mathbf{0}, \mathbf{0}) \le c_1|||(\mathbf{u}, p, \boldsymbol{\sigma}, \boldsymbol{\tau})|||^2,$$

for sufficiently small values of M, $\mathcal{W}]$ and $\mathcal{R}]$.

The proof of this theorem is included Appendix A.

We end this section by detailing the projection of the velocity onto an approximately divergence free subspace of $\mathbf{V}$. Given the current approximation for the velocity, $\mathbf{u}$, we seek to find $\mathbf{b} \in \mathbf{V}$ such that

$$\begin{cases}
\nabla\cdot\mathbf{b} = 0,\\
\nabla\times\mathbf{b} = \nabla\times\mathbf{u}.
\end{cases}$$

This is done by defining

$$G_b(\mathbf{b}; \mathbf{u}) = \|\nabla\cdot\mathbf{b}\|^2 + \|\nabla\times(b-u)\|^2,$$

and finding $\mathbf{b} \in \mathbf{V}$ such that

$$G_b(\mathbf{b}; \mathbf{u}) = \inf_{\mathbf{v}\in\mathbf{V}} G_b(\mathbf{v}; \mathbf{u}).$$

This well-posed div-curl system is well studied in the literature, see for example [7,10].

5. Finite element approximation

The least-squares minimization problem for the solution of system (9) is to choose $(\mathbf{u}, p, \boldsymbol{\sigma}, \boldsymbol{\tau}) \in \mathbf{X}$ such that

$$G(\mathbf{u}, p, \boldsymbol{\sigma}, \boldsymbol{\tau}; \mathbf{f}, \mathbf{F}) = \inf_{(\mathbf{v}, q, \mathbf{s}, \mathbf{t})\in\mathbf{X}} G(\mathbf{v}, q, \mathbf{s}, \mathbf{t}; \mathbf{f}, \mathbf{F}). \tag{10}$$

Let $\mathcal{T}_h$ be a regular triangulation of Ω with a meshsize of $O(h)$. Denoteby $P_k(K)$ the standard space of degree k polynomials on

element K. Also, consider the Raviart–Thomas space of order k on element K defined by

$$RT_k(K) = P_k(K)^d + \mathbf{x}P_k(K),$$

where $\mathbf{x} = (x_1, \ldots, x_d)^t$.

The finite element approximation spaces we consider are continuous piecewise polynomials for $\mathbf{u}$, p and $\boldsymbol{\tau}$, and the $H(\mathrm{div})$ conforming Raviart–Thomas space for $\boldsymbol{\sigma}$ given by:

$$\begin{aligned}
\mathbf{V}^h &= \{\mathbf{v} \in C^0(\Omega)^d : \mathbf{v}|_K \in P_{k+1}(K)^d \forall K \in \mathcal{T}_h, \mathbf{v} = \mathbf{0} \text{ on } \partial\Omega\},\\
\mathbf{Q}^h &= \{q \in C^0(\Omega) : q|_K \in P_{k+1}(K) \forall K \in \mathcal{T}_h\},\\
\mathbf{S}^h &= \{\mathbf{s} \in \mathbf{S} : \mathbf{s}|_K \in RT_k(K) \forall K \in \mathcal{T}_h\},\\
\mathbf{T}^h &= \{\mathbf{t} \in \mathbf{T} \cap C^0(\Omega)^{d\times d} : \mathbf{t} \in P_{k+1}(K)^{d\times d} \quad \forall K \in \mathcal{T}_h\}.
\end{aligned}$$

These spaces satisfy standard approximation properties, which are briefly summarized here. Let scalar ϕ^h represent any of the components in either $\mathbf{V}^h$, $\mathbf{Q}^h$ or $\mathbf{T}^h$, where $\Phi^h = \{\phi \in C^0(\Omega) : \phi|_K \in P_{k+1}(K) \forall K \in \mathcal{T}_h\}$ admits the property

$$\inf_{\phi^h \in \Phi^h} \|\phi - \phi^h\|_\ell \le Ch^m \|\phi\|_{m+\ell} \forall \phi \in H^{m+\ell}(\Omega), \tag{11}$$

for $\ell = 0, 1$ (see e.g. [6]). Space $\mathbf{S}^h$ admits

$$\inf_{\boldsymbol{\sigma} \in \mathbf{S}^h} (\|\boldsymbol{\sigma} - \boldsymbol{\sigma}^h\| + \|\nabla \cdot (\boldsymbol{\sigma} - \boldsymbol{\sigma}^h)\|) \le Ch^m (\|\boldsymbol{\sigma}\|_m + \|\nabla \cdot \boldsymbol{\sigma}\|_m) \tag{12}$$

for $\boldsymbol{\sigma} \in \mathbf{S} \cap H^m(\Omega)^{d\times d}$ with $\nabla \cdot \boldsymbol{\sigma} \in H^m(\Omega)^d$.

The discrete minimization problem is to choose $(\mathbf{u}^h, p^h, \boldsymbol{\sigma}^h, \boldsymbol{\tau}^h) \in \mathbf{X}^h$ such that

$$G(\mathbf{u}^h, p^h, \boldsymbol{\sigma}^h, \boldsymbol{\tau}^h; \mathbf{f}, \mathbf{F}) = \min_{(\mathbf{v}^h, q^h, \mathbf{s}^h, \mathbf{t}^h) \in \mathbf{X}^h} G(\mathbf{v}^h, q^h, \mathbf{s}^h, \mathbf{t}^h; \mathbf{f}, \mathbf{F}). \tag{13}$$

We now give error estimates for the solution to (13).

Theorem 5.1. *Consider approximating the solution to (9) through the discrete minimization problem (13) under the assumptions in (8). Assume that $(\mathbf{u}, p, \boldsymbol{\sigma}, \boldsymbol{\tau}) \in \mathbf{X}$ is the solution to (10), then the solution to (13) satisfies*

$$\begin{aligned}
&|||(\mathbf{u} - \mathbf{u}^h, p - p^h, \boldsymbol{\sigma} - \boldsymbol{\sigma}^h, \boldsymbol{\tau} - \boldsymbol{\tau}^h)|||\\
&\quad \le Ch^m (\|\mathbf{u}\|_{m+1} + \|p\|_m + \|\boldsymbol{\sigma}\|_m + \|\nabla \cdot \boldsymbol{\sigma}\|_m + \|\boldsymbol{\tau}\|_{m+1}),
\end{aligned}$$

for $m \le k+1$.

Proof. Theorem 4.1 directly leads to the bound

$$\begin{aligned}
&|||(\mathbf{u} - \mathbf{u}^h, p - p^h, \boldsymbol{\sigma} - \boldsymbol{\sigma}^h, \boldsymbol{\tau} - \boldsymbol{\tau}^h)|||^2\\
&\quad \le \inf_{(\mathbf{v}^h, q^h, \mathbf{s}^h, \mathbf{t}^h) \in \mathbf{S}^h} \frac{c_1}{c_0} |||(\mathbf{u} - \mathbf{v}^h, p - q^h, \boldsymbol{\sigma} - \mathbf{s}^h, \boldsymbol{\tau} - \mathbf{t}^h)|||^2,
\end{aligned}$$

which, using $\|\mathbf{b}\| \cdot \nabla(\boldsymbol{\tau} - \mathbf{t}^h) \le C\|\nabla(\boldsymbol{\tau} - \mathbf{t}^h)\|$ and the approximation properties in (11) and (12), yield the desired error bound for $m \le k+1$. □

We note that one may use L^2 elements of order k (i.e., lower order than presented above) for the pressure, p, and still achieve the bounds in Theorem 5.1. In practice we prefer to choose the finite element spaces described here.

Here, as in all such finite element simulations, the order of convergence depends on both the order of the finite element spaces used and the smoothness of the solution. Various estimates in [24,33,20] indicate that, at least for small data and smooth domain, system (2) admits full regularity. Thus, we expect any loss of smoothness in the solutions we seek are due to boundary singularities. In Section 6 we detail the method we use to treat boundary singularities.

6. Boundary singularities

In the previous section, the error bounds for the approximated solution are optimal under sufficient regularity of the original problem. However, if the solution has boundary singularities then we may expect a degradation of the discretization rates according to the smoothness of the solution. Assume for the present that Ω is a closed, bounded domain in $\mathbb{R}^2$ with a polygonal corner located at the origin, and that (r, θ) are polar coordinates. In general, second-order, elliptic-like problems with such boundary configurations admit solutions that include a component of the form

$$s(r, \theta) = r^\alpha g(\theta).$$

The power of the singularity, α, depends on the PDE and interior angle of the corner, γ. Substantial literature exists on the singular functions associated with incompressible fluids.

For $\gamma < \pi$ (i.e., non-reentrant corners), [19] shows that solutions have Newtonian behavior. But analytical studies [25,19,22,36] and numerical computations in [27,1] show that for geometries with $\gamma = 3\pi/2$, steady solutions behave as

$$u_i \sim r^{5/9}, \quad \psi \sim r^{14/9}, \quad \text{and} \quad \tau_{ij} \sim r^{-2/3}, \tag{14}$$

where u_i and τ_{ij} are components of the velocity and extra stress, respectively, and ψ is the streamfunction. Thus here we have $\mathbf{u} \notin H^2(\Omega)^2$ and $\boldsymbol{\tau} \notin H^1(\Omega)^{2\times 2}$. This lack of smoothness indicates that using finite element subspaces of $H^1(\Omega)$ for the extra stress may cause unintended difficulties. Theorem 5.1 illustrates this appropriately. In fact, even though this loss of smoothness exists only in the neighborhood of the singular point, it is well known that finite element methods experience a resulting *pollution effect*, that is, significant errors with global support will not be resolvable without directly addressing the singularity. We note that for problems such as this, mesh refinement alone is insufficient to capture errors outside $H^1(\Omega)$.

Many approaches to deal with boundary singularities exist, many of which require precise *a priori* forms of the singular solutions. We use a method developed for least-squares discretizations which requires only a rough approximation of the power of the dominant singularity, and recovers optimal convergence of the method in weighted norms. We summarize the approach briefly here in general notation.

Denote by $LU = f$ the linear system in (9) for which we seek $U = (\mathbf{u}, p, \boldsymbol{\sigma}, \boldsymbol{\tau}) \in \mathbf{X}$ by minimizing the weighted least-squares functional

$$G(U; f) = \|w(LU - f)\|^2.$$

When $w = 1$, this coincides with the description in (4). By choosing an appropriate weight function, w, we seek to eliminate the pollution effect caused by a loss of smoothness in U near boundary singularities. Such weighted-norm least-squares problems are studied in [18,29,30,15], and use

$$w = w(r) = \begin{cases} (r/R)^\beta, & r < R,\\ 1, & r \ge R, \end{cases}$$

where β is chosen so that $wU \in H^2(\Omega)$ and $R \ll \mathrm{diam}(\Omega)$ is chosen to localize the weight function. A simple calculation thus determines the value of β given the power of the singularity in U. For example, the Oldroyd system highlighted in (14) requires $\beta > 5/3$.

7. Numerical experiments

We now consider flow of an Oldroyd-B fluid in a 4:1 planar contraction. In this problem, creeping flow from a channel of large diameter is abruptly constricted to a channel of smaller diameter. The domain is symmetric about the centerline of each channel,

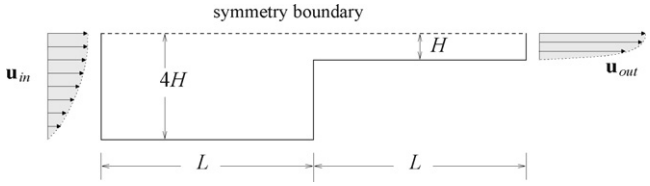

Fig. 2. 4:1 contraction problem.

and for efficiency the computational domain used is one-half of the physical domain. Following standard benchmark solutions (see e.g., [1,27]) for this problem, we use retardation parameter $\omega = 1/9$, Reynolds number $\mathcal{R}\rceil = 0$, and the geometry shown in Fig. 2. For the computations summarized here we use $L = 10$ and $H = 1$. With the origin at the lower left corner of the domain, we choose the velocity boundary conditions on the inflow and outflow boundaries (Γ_{in} and Γ_{out}, respectively) to be

$$u_1 = \frac{3}{128}y(8-y),\ u_2 = 0 \ \text{ on } \ \Gamma_{\text{in}}, \quad \text{and}$$

$$u_1 = \frac{3}{2}(y-3)(5-y),\ u_2 = 0 \ \text{ on } \ \Gamma_{\text{out}}.$$

This scaling ensures a balance of flux in the inlet and outlet and gives a unit average velocity in the fully developed downstream channel. Following the weighted-norm approach described in the previous section, each intermediate step minimizes a linearized, weighted least-squares functional with $\beta = 2.0$ and $R = 1$. We also define the weighted nonlinear functional as in (6), with the same weight function as the linearized functionals.

Numerical results are obtained for $\mathcal{W}\rceil = 0, 1, 2, 3$. Each problem is initially discretized with a regular triangulation of the domain containing 5646 elements, and allowed four adaptive refinement steps according to the nested iteration algorithm described in Section 3. Fig. 3 shows the final mesh and a detail near the reentrant corner. The finite element spaces used are continuous piecewise linears, P_1, for u, p and $\boldsymbol{\tau}$ and the lowest-order Raviart–Thomas elements, RT_0, for the total stress, $\boldsymbol{\sigma}$.

Fig. 3 shows the final mesh for $\mathcal{W}\rceil = 1$, $\mathcal{R}\rceil = 10$, which shows that mesh refinement is concentrated near the reentrant corner and the downstream boundary layer. We note that, for this problem, the symmetry boundary condition is imposed weakly by the addition of an extra term in the least-squares functional. Because of this the symmetry boundary tends also to be refined in this test problem.

The resulting elastic stress fields are shown in Fig. 4. Dimensionless stresses are normalized by $\mu V/H$, where $\mu = \mu_1 + \mu_2$ is the total viscosity, V is the average horizontal velocity at the outflow boundary, and H is the radius of the downstream channel. The qualitative nature of the solution is consistent with the existing literature for this model problem, showing strong singularities at the reentrant corner and pronounced downstream stress boundary layers.

To illustrate convergence of the method and validate the theoretical results of this paper, Table 1 shows reduction of the nonlinear functional norm, $\mathcal{G}^{1/2}$, with increasing resolution for different Weissenberg and Reynolds numbers. Here, N denotes the total number of elements and *steps* is the number of Newton steps used on the current mesh level. For the finite element spaces used here, optimal convergence implies

$$\mathcal{G}^{1/2} = O(N^{-1/2}).$$

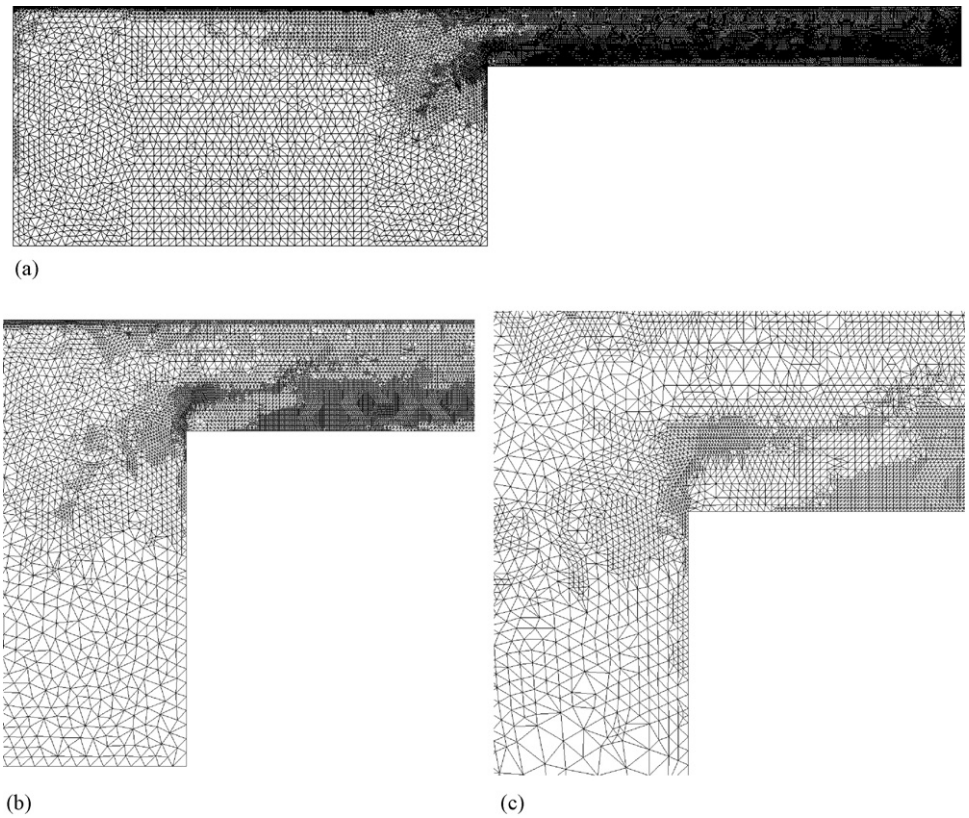

Fig. 3. Final mesh after four refinement steps: full domain and details near the reentrant corner for $\mathcal{W}e = 1$, $\mathcal{R}e = 10$. (a) Full computational domain, $(x, y) \in [0, 16] \times [0, 4]$. (b) Detail for $(x, y) \in [6.4, 10.6] \times [0, 4]$. (c) Detail for $(x, y) \in [7.1, 9.2] \times [1.8, 3.8]$.

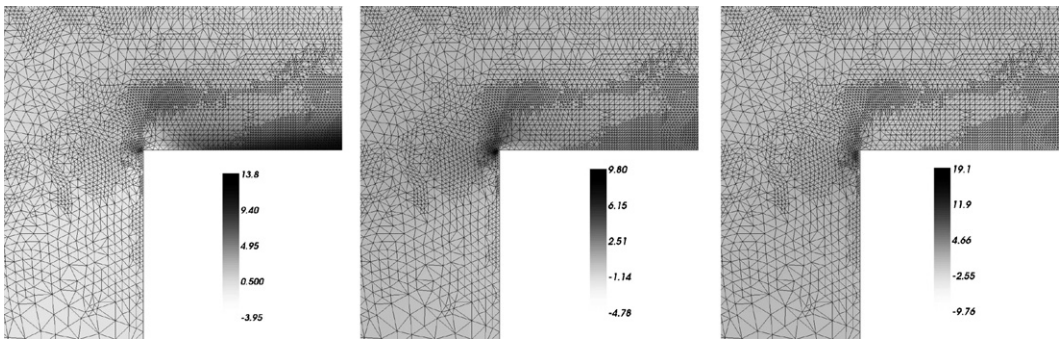

Fig. 4. Elastic stresses, τ_{11}, τ_{12}, and τ_{22} near the reentrant corner for $\mathcal{W}e = 1$, $\mathcal{R}e = 10$.

To monitor the convergence, define the discretization efficiency by

$$\text{Eff} = \frac{\mathcal{G}_{\text{old}}^{1/2}/\mathcal{G}_{\text{new}}^{1/2}}{N_{\text{new}}^{1/2}/N_{\text{old}}^{1/2}}.$$

Thus optimal convergence yields Eff = 1, and Table 1 shows that functional convergence is fairly robust with respect to the Weissenberg and Reynolds numbers. The same data is also summarized in Fig. 5.

In Fig. 6 we report asymptotic behavior at the reentrant corner. Analytical results in [25,19,22,36] suggest that for this geometry the local behavior of the velocity follows $u_i \sim r^{5/9}$ (for $i = 1, 2$) and the streamfunction follows $\psi \sim r^{14/9}$. The velocity components and streamfunction are shown in a log scale plot in Fig. 6, and the expected asymptotic slopes are included for reference. Data is sampled along a line with angle $\theta = \pi/2$ from the downstream wall.

In addition to the reduction of the functional at expected rates, we compare our numerical results to benchmark solutions by Alves et al. [1] and Kim et al. [27]. Table 2 reports the horizontal reattachment length (denoted by X_R as in Fig. 2) of the salient corner vortex for increasing $\mathcal{W}$], $\omega = 1/9$ and $\mathcal{R}$] = 0. Our results compare well with benchmark solutions, generally matching the expected trend of the vortex size. Alves et al. gives detailed further comparison with earlier works on reattachment lengths in [1].

Table 1
Reduction of the nonlinear functional norm in nonlinear nested iteration for various Weissenberg numbers and Reynolds numbers.

N	Steps	$\mathcal{G}^{1/2}$	Eff	N	Steps	$\mathcal{G}^{1/2}$	Eff
$\mathcal{W}$] = 0, $\mathcal{R}$] = 0				$\mathcal{W}$] = 0, $\mathcal{R}$] = 10			
5660	1	1.206		5660	2	1.260	
10457	1	0.847	1.05	10082	2	0.891	1.06
21733	1	0.638	0.92	20789	2	0.670	0.93
41704	1	0.478	0.96	47807	1	0.488	0.90
$\mathcal{W}$] = 1, $\mathcal{R}$] = 0				$\mathcal{W}$] = 1, $\mathcal{R}$] = 10			
5660	3	1.605		5660	4	1.608	
10509	2	1.096	1.08	11420	2	1.133	1.00
18914	2	0.810	1.01	22716	2	0.806	1.00
35765	1	0.608	0.97	53019	1	0.572	0.92
$\mathcal{W}$] = 2, $\mathcal{R}$] = 0				$\mathcal{W}$] = 2, $\mathcal{R}$] = 10			
5660	3	2.878		5660	3	2.895	
10378	3	1.014	2.10	11620	3	1.033	1.96
18734	2	0.791	0.95	23020	2	0.820	0.89
33849	2	0.655	0.90	50882	2	0.671	0.82
$\mathcal{W}$] = 3, $\mathcal{R}$] = 0				$\mathcal{W}$] = 3, $\mathcal{R}$] = 10			
5660	3	3.979		5660	3	4.101	
10224	3	0.840	3.52	12143	3	0.854	3.28
19548	2	0.699	0.87	23816	2	0.712	0.86
36607	2	0.579	0.88	53610	2	0.597	0.80

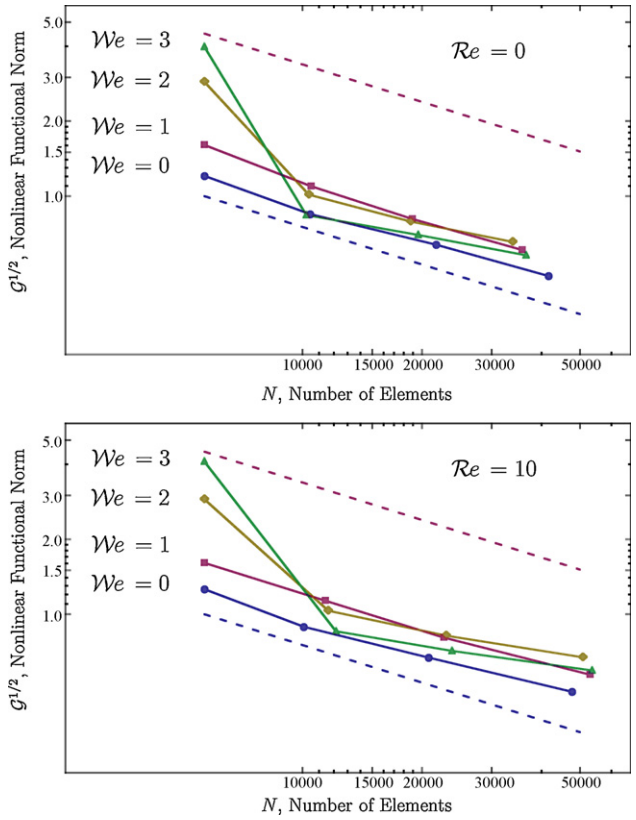

Fig. 5. Reduction of nonlinear functional norm vs. total number of elements. The slope of the dashed lines indicate the asymptotic optimal rate.

In summary we have presented a least-squares finite element approach to the Oldroyd model for viscoelastic fluids, which makes use of a nonlinear functional to adaptively refine the mesh. For the test problem considered, the refinement that results is of good quality and refinement is concentrated near the reentrant corner and downstream boundary layers. Our convergence theory and numerical results are in good agreement, as shown by the reduction of the

Table 2
Reattachment lengths, X_R, of the salient corner recirculation with $\mathcal{R}e = 0$, compared with benchmark solutions in [1,27].

X_R			
$\mathcal{W}e$	This work	Alves et al.	Kim et al.
0.0	1.560	1.502	1.4481
1.0	1.499	1.373	1.3392
2.0	1.200	1.181	1.1245
3.0	1.059	0.973	0.9001

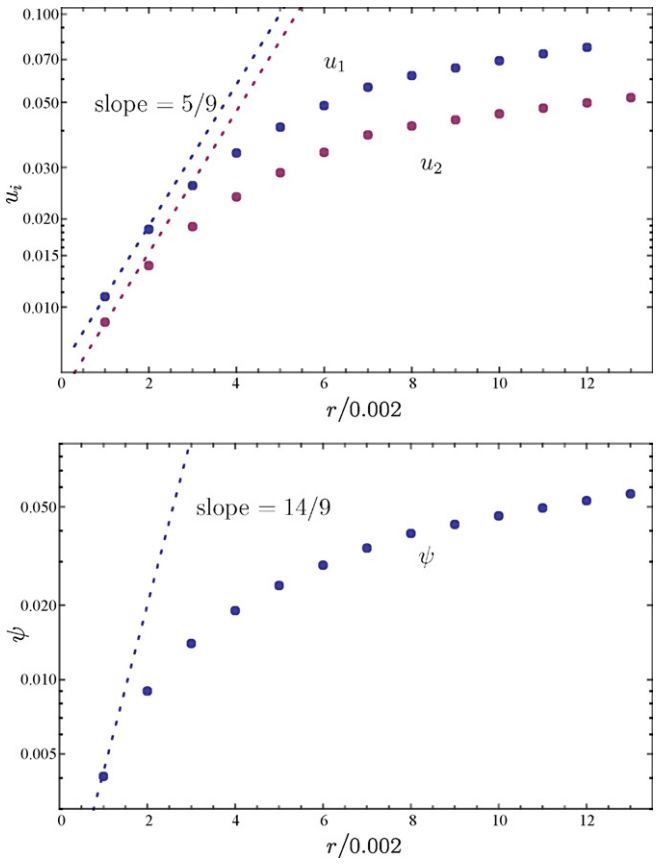

Fig. 6. Asymptotic behavior of the velocity and streamfunction near the reentrant corner for $\mathcal{W}e = 1$, $\mathcal{R}e = 0$. Data is sampled along a line at $\theta = \pi/2$ from the downstream wall (c.f. Fig. 2).

nonlinear functional norm. Our results also compare favorably with established benchmark solutions.

Appendix A. Proof of thm:ellipticityTheorem 4.1

Proof. The upper bound follows naturally from the triangle inequality and (8). For the lower bound we first show

$$|||(\mathbf{u}, p, \boldsymbol{\sigma}, \boldsymbol{\tau})|||^2 \le C\mathcal{F}, \tag{A.1}$$

where

$$\mathcal{F} := \|\nabla\cdot\mathbf{u}\|^2 + \|\nabla\cdot\boldsymbol{\sigma}\|^2 + \|\boldsymbol{\sigma} - \boldsymbol{\tau} + p\mathbf{I} - 2(1-\omega)\boldsymbol{\epsilon}(\mathbf{u})\|^2 + \|\boldsymbol{\tau} + \mathcal{W}]\mathbf{b}\cdot\nabla\boldsymbol{\tau} - 2\omega\boldsymbol{\epsilon}(\mathbf{u})\|^2.$$

We rely on the following standard Korn and Poincaré inequalities:

$$\|\nabla\mathbf{u}\| \le C\|\boldsymbol{\epsilon}(\mathbf{u})\|, \tag{A.2}$$

$$\|\mathbf{u}\|_1 \le C\|\nabla\mathbf{u}\|. \tag{A.3}$$

As in [13] we define the fourth-order compliance tensor $\mathcal{A} : \mathbb{R}^{d\times d} \to \mathbb{R}^{d\times d}$ by

$$\mathcal{A}\boldsymbol{\tau} = \boldsymbol{\tau} - \frac{1}{d}\mathrm{tr}(\boldsymbol{\tau})\mathbf{I} \quad \forall\boldsymbol{\tau}\in\mathbb{R}^{d\times d}.$$

Since $\mathcal{A}\boldsymbol{\sigma}$ is trace-free, we have $\langle\mathcal{A}\boldsymbol{\sigma}, p\mathbf{I}\rangle = 0$ and $\langle\mathcal{A}\boldsymbol{\sigma}, \mathcal{A}\boldsymbol{\sigma}\rangle = \langle\mathcal{A}\boldsymbol{\sigma}, \boldsymbol{\sigma}\rangle$, and from [13], for all $\boldsymbol{\sigma}\in\mathbf{S}$ we have the inequality

$$\|\mathrm{tr}(\boldsymbol{\sigma})\| \le C(\|\mathcal{A}\boldsymbol{\sigma}\| + \|\nabla\cdot\boldsymbol{\sigma}\|) \tag{A.4}$$

(actually, a stronger result is proved there, but this result is sufficient for the present purposes). Further, wenote that the Cauchy–Schwarz inequality leads to

$$\begin{aligned}\|\mathcal{A}\boldsymbol{\sigma}\|^2 &= \langle\mathcal{A}\boldsymbol{\sigma}, \boldsymbol{\sigma}\rangle = \langle\mathcal{A}\boldsymbol{\sigma}, \boldsymbol{\sigma} - \boldsymbol{\tau} + p\mathbf{I} - 2(1-\omega)\boldsymbol{\epsilon}(\mathbf{u})\rangle\\ &\quad + \langle\mathcal{A}\boldsymbol{\sigma}, \boldsymbol{\tau}\rangle + \langle\mathcal{A}\boldsymbol{\sigma}, 2(1-\omega)\boldsymbol{\epsilon}(\mathbf{u})\rangle \le \|\mathcal{A}\boldsymbol{\sigma}\|(\|\boldsymbol{\sigma} - \boldsymbol{\tau}\\ &\quad + p\mathbf{I} - 2(1-\omega)\boldsymbol{\epsilon}(\mathbf{u})\| + \|\boldsymbol{\tau}\| + 2(1-\omega)\|\boldsymbol{\epsilon}(\mathbf{u})\|).\end{aligned}$$

From this and (A.4) it then follows that

$$\|\mathrm{tr}(\boldsymbol{\sigma})\| \le C(\|\mathcal{A}\boldsymbol{\sigma}\| + \|\nabla\cdot\boldsymbol{\sigma}\|) \le C(\mathcal{F}^{1/2} + \|\boldsymbol{\tau}\| + \|\boldsymbol{\epsilon}(\mathbf{u})\|).$$

The pressure may now be bounded by

$$\begin{aligned}\|p\| &\le \|\mathrm{tr}(\boldsymbol{\sigma} - \boldsymbol{\tau} + p\mathbf{I} - 2(1-\omega)\boldsymbol{\epsilon}(\mathbf{u}))\| + \|\mathrm{tr}(\boldsymbol{\sigma})\| + \|\mathrm{tr}(\boldsymbol{\tau})\|\\ &\quad + 2(1-\omega)\|\boldsymbol{\epsilon}(\mathbf{u})\| \le C(\mathcal{F}^{1/2} + \|\boldsymbol{\tau}\| + \|\boldsymbol{\epsilon}(\mathbf{u})\|),\end{aligned} \tag{A.5}$$

and, similarly, we have

$$\begin{aligned}\|\mathbf{b}\cdot\nabla\boldsymbol{\tau}\| &\le C(\|\boldsymbol{\tau} + \mathcal{W}e\mathbf{b}\cdot\nabla\boldsymbol{\tau} - 2\omega\boldsymbol{\epsilon}(\mathbf{u})\| + \|\boldsymbol{\tau}\| + 2\omega\|\boldsymbol{\epsilon}(\mathbf{u})\|)\\ &\le C(\mathcal{F}^{1/2} + \|\boldsymbol{\tau}\| + \|\boldsymbol{\epsilon}(\mathbf{u})\|).\end{aligned} \tag{A.6}$$

We also write

$$\begin{aligned}4\omega(1-\omega)\|\boldsymbol{\epsilon}(\mathbf{u})\|^2 &= \langle-\boldsymbol{\sigma} + \boldsymbol{\tau} - p\mathbf{I} + 2(1-\omega)\boldsymbol{\epsilon}(\mathbf{u}), 2\omega\boldsymbol{\epsilon}(\mathbf{u})\rangle\\ &\quad + 2\omega\langle\boldsymbol{\sigma}, \boldsymbol{\epsilon}(\mathbf{u})\rangle - 2\omega\langle\boldsymbol{\tau}, \boldsymbol{\epsilon}(\mathbf{u})\rangle + 2\omega\langle p\mathbf{I}, \boldsymbol{\epsilon}(\mathbf{u})\rangle,\end{aligned} \tag{A.7}$$

and note that, since $\nabla\cdot\mathbf{b} = \mathbf{0}$ and $\mathbf{b}|_{\partial\Omega} = \mathbf{0}$, we also have

$$\begin{aligned}\langle\mathbf{b}\cdot\nabla\tau_{ij}, \tau_{ij}\rangle &= -\langle\tau_{ij}, \nabla\cdot(\mathbf{b}\tau_{ij})\rangle\\ &= -\langle\tau_{ij}, (\nabla\cdot\mathbf{b})\tau_{ij} + \mathbf{b}\cdot\nabla\tau_{ij}\rangle = -\langle\tau_{ij}, \mathbf{b}\cdot\nabla\tau_{ij}\rangle,\end{aligned}$$

which implies $\langle\mathbf{b}\cdot\nabla\boldsymbol{\tau}, \boldsymbol{\tau}\rangle = 0$ and thus

$$\|\boldsymbol{\tau}\|^2 = \langle\boldsymbol{\tau} + \mathcal{W}e\mathbf{b}\cdot\nabla\boldsymbol{\tau} - 2\omega\boldsymbol{\epsilon}(\mathbf{u}), \boldsymbol{\tau}\rangle + 2\omega\langle\boldsymbol{\epsilon}(\mathbf{u}), \boldsymbol{\tau}\rangle. \tag{A.8}$$

Using symmetry, we note that

$$\begin{aligned}\|\boldsymbol{\sigma} - \boldsymbol{\sigma}^t\| &= \|\boldsymbol{\sigma} - \boldsymbol{\tau} + p\mathbf{I} - 2(1-\omega)\boldsymbol{\epsilon}(\mathbf{u})\\ &\quad - (\boldsymbol{\sigma} - \boldsymbol{\tau} + p\mathbf{I} - 2(1-\omega)\boldsymbol{\epsilon}(\mathbf{u}))^t\|\\ &\le 2\|\boldsymbol{\sigma} - \boldsymbol{\tau} + p\mathbf{I} - 2(1-\omega)\boldsymbol{\epsilon}(\mathbf{u})\| \le 2\mathcal{F}^{1/2},\end{aligned}$$

which leads to

$$\begin{aligned}|\langle\boldsymbol{\sigma}, \boldsymbol{\epsilon}(\mathbf{u})\rangle| &= \left|\left\langle\boldsymbol{\sigma}, \frac{1}{2}(\nabla\mathbf{u} + \nabla\mathbf{u}^t)\right\rangle\right|\\ &= \left|\left\langle\frac{1}{2}(\boldsymbol{\sigma} + \boldsymbol{\sigma}^t), \nabla\mathbf{u}\right\rangle\right|\\ &= \left|\langle\boldsymbol{\sigma}, \nabla\mathbf{u}\rangle - \left\langle\frac{1}{2}(\boldsymbol{\sigma} - \boldsymbol{\sigma}^t), \nabla\mathbf{u}\right\rangle\right|\\ &= \left|-\langle\nabla\cdot\boldsymbol{\sigma}, \mathbf{u}\rangle - \frac{1}{2}\langle\boldsymbol{\sigma} - \boldsymbol{\sigma}^t, \nabla\mathbf{u}\rangle\right|\\ &\le \mathcal{F}^{1/2}\|\mathbf{u}\| + \frac{1}{2}\|\boldsymbol{\sigma} - \boldsymbol{\sigma}^t\|\|\nabla\mathbf{u}\| \le \mathcal{F}^{1/2}\|\mathbf{u}\|_1.\end{aligned} \tag{A.9}$$

Combining (A.7) and (A.8), and using (A.9), the Cauchy–Schwarz inequality, and the general relation, $2ab \le \delta^{-1}a^2 + \delta b^2$, we bound the linear combination

$$\begin{aligned}4\omega(1-\omega)\|\boldsymbol{\epsilon}(\mathbf{u})\|^2 + \|\boldsymbol{\tau}\|^2 &= \langle-\boldsymbol{\sigma} + \boldsymbol{\tau} - p\mathbf{I} + 2(1-\omega)\boldsymbol{\epsilon}(\mathbf{u}), 2\omega\boldsymbol{\epsilon}(\mathbf{u})\rangle\\ &\quad + 2\,\omega\langle p, \nabla\cdot\mathbf{u}\rangle + 2\omega\langle\boldsymbol{\sigma}, \boldsymbol{\epsilon}(\mathbf{u})\rangle\\ &\quad + \langle\boldsymbol{\tau} + \mathcal{W}]\mathbf{b}\cdot\nabla\boldsymbol{\tau} - 2\omega\boldsymbol{\epsilon}(\mathbf{u}), \boldsymbol{\tau}\rangle\\ &\le C\left(\delta + \frac{1}{\delta}\right)\mathcal{F} + C\delta(\|\boldsymbol{\epsilon}(\mathbf{u})\|^2 + \|\boldsymbol{\tau}\|^2),\end{aligned}$$

for any $\delta > 0$. By choosing δ sufficiently small, we immediately have that

$$\|\boldsymbol{\epsilon}(\mathbf{u})\|^2 + \|\boldsymbol{\tau}\|^2 \leq C\mathcal{F},$$

which, with (A.5), (A.6), (A.2) and (A.3), establishes (A.1).

We now may use (8) and the inequality $\|a+b\|^2 \geq (1/2)\|a\|^2 - \|b\|^2$ to get

$$\begin{aligned}
G(\mathbf{u}, p, \boldsymbol{\sigma}, \boldsymbol{\tau}; \mathbf{0}, \mathbf{0}) &= \|\nabla \cdot \mathbf{u}\|^2 + \|\boldsymbol{\sigma} - \boldsymbol{\tau} + p\mathbf{I} - 2(1-\omega)\boldsymbol{\epsilon}(\mathbf{u})\|^2 \\
&\quad + \|\mathcal{R}\rceil(\mathbf{b}\cdot\nabla\mathbf{u} + \mathbf{u}\cdot\nabla\mathbf{b}) - \nabla\cdot\boldsymbol{\sigma}\|^2 \\
&\quad + \|\boldsymbol{\tau} + \mathcal{W}\rceil\mathbf{b}\cdot\nabla\boldsymbol{\tau}^2 + B(\mathbf{u}, \boldsymbol{\tau}) - 2\omega\boldsymbol{\epsilon}(\mathbf{u})\|^2 \\
&\geq \|\nabla \cdot \mathbf{u}\|^2 + \|\boldsymbol{\sigma} - \boldsymbol{\tau} + p\mathbf{I} - 2(1-\omega)\boldsymbol{\epsilon}(\mathbf{u})\|^2 \\
&\quad + \frac{1}{2}\|\nabla\cdot\boldsymbol{\sigma}\|^2 - \|\mathcal{R}\rceil(\mathbf{b}\cdot\nabla\mathbf{u} + \mathbf{u}\cdot\nabla\mathbf{b})\|^2 \\
&\quad + \frac{1}{2}\|\boldsymbol{\tau} + \mathcal{W}\rceil\mathbf{b}\cdot\nabla\boldsymbol{\tau} - 2\omega\boldsymbol{\epsilon}(\mathbf{u})\|^2 - \|B(\mathbf{u}, \boldsymbol{\tau})\|^2 \\
&\geq \frac{1}{2}\mathcal{F} - C\mathcal{R}\rceil^2 M^2\|\mathbf{u}\|_1^2 - C\mathcal{W}\rceil^2 M^2(\|\mathbf{u}\|_1^2 + \|\boldsymbol{\tau}\|^2) \\
&\geq C(|||(\mathbf{u}, p, \boldsymbol{\sigma}, \boldsymbol{\tau})|||^2 - \mathcal{R}\rceil^2 M^2\|\mathbf{u}\|_1^2 \\
&\quad - \mathcal{W}\rceil^2 M^2(\|\mathbf{u}\|_1^2 + \|\boldsymbol{\tau}\|^2)) \\
&\geq c_0|||(\mathbf{u}, p, \boldsymbol{\sigma}, \boldsymbol{\tau})|||^2
\end{aligned}$$

where $c_0 > 0$ for M, $\mathcal{R}\rceil$ and $\mathcal{W}\rceil$ chosen sufficiently small. □

References

[1] M. Alves, P. Oliveira, F. Pinho, Benchmark solutions for the flow of oldroyd-b and ptt fluids in planar contractions, J. Non-Newt. Fluid Mech. 110 (2003) 45–75.
[2] G. Astarita, G. Marrucci, Principles on Non-Newtonian Fluid Mechanics, McGraw Hill, New York, 1974.
[3] P. Bochev, M. Gunzburger, Analysis of least-squares finite element methods for the stokes equations, Math. Comp. 63 (1994) 479–506.
[4] P. Bochev, M. Gunzburger, Finite element methods of least-squares type, SIAM Rev. 40 (1998) 789–837.
[5] A. Bose, G. Carey, Least-squares p-r finite element methods for incompressible non-Newtonian flows, Comput. Method Appl. M. 180 (1999) 431–458.
[6] D. Braess, Finite Elements: Theory, Fast Solvers and Applications in Solid Mechanics, Cambridge, 2001.
[7] Z. Cai, R. Lazarov, T. Manteuffel, S. McCormick, First-order system least squares for second-order partial differential equations: Part I, SIAM J. Numer. Anal. 31 (1994) 1785–1799.
[8] Z. Cai, B. Lee, P. Wang, Least-squares methods for incompressible newtonian fluid flow: linear stationary problems, SIAM J. Numer. Anal. 42 (2004) 843–859.
[9] Z. Cai, C.-O. Lee, T. Manteuffel, S. McCormick, First-order system least squares for linear elasticity: numerical results, SIAM J. Sci. Comput. 21 (2000) 1706–1727.
[10] Z. Cai, T. Manteuffel, S. McCormick, First-order system least squares for second-order partial differential equations: Part II, SIAM J. Numer. Anal. 34 (1997) 425–454.
[11] Z. Cai, T. Manteuffel, S. McCormick, First-order system least squares for the stokes equations, with application to linear elasticity, SIAM J. Numer. Anal. 34 (1997) 1727–1741.
[12] Z. Cai, T. Manteuffel, S. McCormick, First-order system least squares for velocity–vorticity–pressure form of the stokes equations, with application to linear elasticity, Elect. Trans. Numer. Anal. 3 (1997) 150–159.
[13] Z. Cai, G. Starke, First-order system least squares for the stress–displacement formulation: linear elasticity, SIAM J. Numer. Anal. 41 (2003) 715–730.
[14] Z. Cai, G. Starke, Least squares methods for linear elasticity, SIAM J. Numer. Anal. 42 (2004) 826–842.
[15] Z. Cai, C. Westphal, A weighted h(div) least-squares method for second-order elliptic problems, SIAM J. Numer. Anal. 46 (2008) 1640–1651.
[16] Z. Cai, S. Zhang, Recovery-based error estimators for interface problems: conforming linear elements, manuscript under review.
[17] A. Codd, T. Manteuffel, S. McCormick, Multilevel first-order system least squares for nonlinear elliptic partial differential equations, SIAM J. Numer. Anal. 41 (2003) 2197–2209.
[18] C. Cox, G. Fix, On the accuracy of least squares methods in the presence of corner singularities, Comput. Math. Appl. 10 (1984) 463–475.
[19] A. Davies, J. Devlin, On corner flows of oldroyd-b fluids, J. Non-Newt. Fluid Mech. 50 (1993) 173–191.
[20] E. Fernández-Cara, F. Guillén, R. Ortega, Some theoretical results concerning non Newtonian fluids of the oldroyd kind, Ann. Scuola. Norm. Sup. Pisa Cl. Sci. 26 (4) (1998) 1–29.
[21] E. Fernández-Cara, F. Guillén, R. Ortega, Mathematical modeling and analysis of viscoelastic fluids of the oldroyd kind, in: P.G. Ciarlet (Ed.), in: Handbook of Numerical Analysis, vol. VIII, Elsevier, 2002, pp. 543–661.
[22] M. Fontelos, A. Friedman, The flow of a class of oldroyd fluids around a reentrant corner, J. Non-Newt. Fluid Mech. 95 (2000) 185–198.
[23] M. Gerritsma, Direct minimization of the discontinuous least-squares spectral element method for viscoelastic fluids, J. Sci. Comput. 27 (2006) 245–256.
[24] C. Guillope, J.-C. Saut, Existence results for the flow of viscoelastic fluids with a differential constitutive law, J. Nonlinear Anal. 15 (1990) 849–869.
[25] E. Hinch, The flow of an oldroyd fluid around a sharp corner, J. Non-Newt. Fluid Mech. 50 (1993) 161–171.
[26] B. Jiang, The Least-squares Finite Element Method, Springer, 1998.
[27] J. Kim, C. Kim, J. Kim, C. Chung, K. Ahn, S. Lee, High-resolution finite element simulation of 4:1 planar contraction flow of viscoelastic fluid, J. Non-Newt. Fluid Mech. 129 (2005) 23–37.
[28] S. Kim, C.-O. Lee, T. Manteuffel, S. McCormick, O. Röhrle, First-order system least squares for the oseen equations, J. Numer. Lin. Alg. Appl. 13 (2006) 461–486, manuscript.
[29] E. Lee, T. Manteuffel, C. Westphal, Weighted-norm first-order system least squares (fosls) for problems with corner singularities, SIAM J. Numer. Anal. 44 (2006) 1974–1996.
[30] E. Lee, T. Manteuffel, C. Westphal, Weighted-norm first-order system least squares (fosls) for div/curl systems with three dimensional edge singularities, SIAM J. Numer. Anal. 46 (2008) 1619–1639.
[31] J. Lions, E. Magenes, Non-Homogenous Boundary Value Problems and Applications, I, Springer-Verlag, New York, 1972.
[32] S. McCormick, T. Manteuffel, J. Schmidt, C. Westphal, First-order system least squares (fosls) for geometrically nonlinear elasticity, SIAM J. Numer. Anal. 44 (2006) 2057–2081.
[33] L. Molinet, R. Talhouk, On the global and periodic regular flows of viscoelastic fluids with a differential constitutive law, NoDEA Nonlin. Differ. Equat. Appl. 11 (2004) 349–359.
[34] J. Oldroyd, On the formation of rheological equations of state, Proc. Roy. Soc. Lond. Ser. A 200 (1950) 523–541.
[35] A. Pipkin, Lectures on Viscoelasticity Theory, 2nd ed., Springer-Verlag, Berlin, 1986.
[36] J. Rallison, E. Hinch, The flow of an oldroyd fluid past a reentrant corner: the downstream boundary layer, J. Non-Newt. Fluid Mech. 116 (2004) 141–162.
[37] M. Renardy, W. Hrusa, J. Nohel, Mathematical Problems in Viscoelasticity, New York, 1987.
[38] G. Starke, An adaptive least-squares mixed finite element method for elasto-plasticity, SIAM J. Numer. Anal. 45 (2007) 371–388.
[39] K. Wang, G. Carey, A least squares finite element method for viscoelastic fluid flow problems, Int. J. Numer. Meth. Fl. 17 (1993) 943–953.